DEVELOPMENT OF HIGH CREEP STRENGTH AND CORROSION-RESISTANT STAINLESS STEELS

B. A. Pint and P. J. Maziasz
Metals and Ceramics Division
Oak Ridge National Laboratory
Oak Ridge, TN 37831-6156

ABSTRACT

Type 347 stainless steel foils are commonly used in primary surface recuperators of gas turbines at gas inlet temperatures up to 600°C. At higher temperatures, accelerated attack due to water vapor in the exhaust gas limits performance. Therefore, new low-cost alternative alloys are being developed with sufficient creep and corrosion resistance at 700°C. The laboratory creep and corrosion performance of an initial attempt at a Fe-20Cr-20Ni-base alloy are presented. The addition of 4Mn in this alloy was successful in preventing accelerated attack at 650-700°C; however, it significantly increased the overall oxidation rate and this likely will lead to a long-term durability problem for thin sections of this material.

Keywords: Stainless steel, gas turbines, recuperators, water vapor, alloy composition

INTRODUCTION

For the past five years, there has been an intensive effort to develop a cost-effective replacement for type 347 stainless steel for higher temperature operation of recuperators or heat exchangers.[1-7] It was determined that type 347, like similar composition 300-series stainless steels, is susceptible to accelerated oxidation attack (AA) in exhaust gas at >600°C due to water vapor, and that more highly alloyed steels are more resistant in this environment.[3,5-12] Switching to a Ni-base alloy, like alloy 625 (Ni-22Cr-9Mo), was appropriate for the recuperator in the Solar Turbine Inc. 4MW Mercury 50 gas turbine.[13] This change can increase recuperator operating temperatures into the 650-700°C range for an overall efficiency of 38.5%. However, for small (30-250kW) single-shaft, gas turbine engines or microturbines,[14] initial cost is a more significant issue and a Ni-base alloy may be prohibitively expensive. Therefore, work has focused on Fe-base alloys, such as NF709 (Fe-20Cr-25Ni),[7,15] as a more cost effective replacement. Work on model alloys[5,6,11] suggested that an Fe-20Cr-20Ni-base alloy may provide sufficient oxidation resistance for this application at an even lower cost. Therefore, alloy development work is examining methods for improving the creep strength of this alloy while maintaining

the corrosion resistance. For a primary surface recuperator,[2,4,7,13] creep strength also is an important issue; however, for plate and fin recuperators,[16] this is less of a concern. This paper presents creep and corrosion results on the first attempt at a strengthened version of this base alloy.

EXPERIMENTAL PROCEDURE

The Fe-20Cr-20Ni-4Mn alloy, along with other model alloys, was vacuum induction melted at Oak Ridge National Laboratory (ORNL) and hot and cold rolled to 0.8mm sheet. After the final cold rolling step, the model alloy sheets were annealed in Ar for 2min at 1000°C and the Fe-20Cr-20Ni-4Mn sheet was annealed for 5min at 1000°C. This produced a 55±10μm grain size (Figure 1a). The sheet was then reduced to 100μm foil by a series of cold rolls and anneals. A final anneal of 5min at 1000°C resulted in a finer grain size of 10±3μm (Figure 1b) compared to the sheet material. Commercial foil materials or commercial alloys rolled to foil at ORNL by a similar process also were studied. The chemical compositions and grain sizes of all of the alloys are listed in Table 1 in order to indicate typical concentrations relative to the nominal values and impurity levels. Oxidation coupons were typically 12mm x 17mm. Sheet specimens were polished to a 600 grit finish while foil specimens were left in the as-rolled surface finish. Prior to oxidation, the specimens were cleaned in acetone and methanol and mass changes were measured using a Mettler-Toledo model AG245 balance after each 100h cycle at 650°, 700° or 800°C.

Oxidation exposures were conducted in laboratory air and humid (10vol.% H_2O) air by flowing the gas at 450cc/min through an alumina tube that was inside a resistively-heated horizontal tube furnace. Distilled water was atomized into the flowing gas stream above its condensation temperature and heated to the reaction temperature within the alumina tube.[1,12] (The effect of water vapor on a particular alloy is a function of a number of variables including test temperature, water content and gas velocity.[1,8,10] For this work, the gas composition and velocity were held constant and temperature was the primary variable.) Up to 40 specimens were positioned in alumina boats in the furnace hot zone so as to expose the specimen faces parallel to the flowing gas. Cycle time at temperature was 100h or 500h. After oxidation, selected specimens were Cu-plated and sectioned for metallographic analysis. Chemical composition was determined using a JEOL 8200 electron microprobe (EPMA) equipped with a wavelength dispersive spectrometer.

RESULTS

To put the effect of water vapor on oxidation resistance in perspective, Figure 2 shows the small mass gains observed for type 347 and 20/25/Nb foils exposed for 40,000-50,000h in laboratory air at 650°C. The data were plotted versus the square root of time to show the parabolic scale growth relationship for the thin protective oxide formed in this test. Figure 3a shows the scale formed on commercial type 347 stainless steel foil after 40,000h at 650°C in laboratory air. The addition of 10% H_2O to the test would result in AA in less than 2,000h.[1,3,9,10]

Previous work on model austenitic and ferritic alloys showed that higher Cr and Ni contents were needed to prevent or delay the onset of AA and that minor additions of Mn and Si were two of the most beneficial elements.[5,12] The minimum Cr and Ni contents needed to be meet a 40,000h service goal in this application appeared to be 20%. (By minimizing the Cr and Ni content in the type 347 replacement alloy, the cost of this component may be kept to a minimum while also meeting the durability goal.) Thus the next step in the development process was to develop an alloy with both adequate corrosion and creep resistance. A combination of Nb, Co, Cu, Mn and N was added to achieve this objective (Table 1). A similar alloying strategy was used to improve the strength of type 347 stainless steel.[2,4] (While the

strength of type 347 was significantly improved by this strategy and the corrosion resistance was improved at 650°C, it was not improved at 700°C significantly.) The creep strength of Fe-20Cr-20Ni-4Mn sheet was compared to commercial and other developmental alloys in a 750°C, 100MPa screening test, Figure 4. The current material showed adequate strength for this application, with a slight improvement over commercial 347 sheet material but was not as strong as the modified 347 compositions.[2,4] As the Fe-20Cr-20Ni-4Mn met the strength goal, it was rolled to 100µm foil for corrosion testing at 650°-800°C.

Results at 650°C

Figure 5 shows specimen mass gain results during 100 h cycles for two Fe-20Cr-20Ni-4Mn foil specimens tested to 6,000 h at 650°C in humid air. For comparison, the results for a number of commercial compositions also are included. Type 347 showed the high mass gain associated with AA after <2,000 h in this test. The mass gains for 20/25/Nb, 120 and 625 all were relatively low, although 20/25/Nb and alloy 120 showed increases after 8,000 h of exposure. These increases were associated with some Fe-rich oxide nodule formation due to Cr depletion on grain boundaries in the substrate.[17] Compared to the higher-alloyed commercial materials, the mass gain for Fe-20Cr-20Ni-4Mn was higher, especially with the >0.1mg/cm^2 gained during the first cycle. A sheet specimen of Fe-20Cr-20Ni-4Mn tested for 10,000 h at this temperature did not show this high transient-stage mass gain but reached a mass gain similar to the foil material by 3,000 h. This specimen showed no signs of AA after 10,000 h and was removed from the test.

None of the long term Fe-20Cr-20Ni-4Mn specimens have been sectioned yet. However, Figures 3b and 3c show the scale formed on Fe-20Cr-20Ni-4Mn foil after 1,000 h (10, 100 h cycles) in humid air. A few Fe-rich nodules formed at the specimen surface. Based on the high initial mass gain, this likely occurred during the first 100 h cycle. However, based on the relatively low subsequent mass change, the nodules did not appear to grow significantly. For comparison, Figure 3d shows the scale formed on Fe-20Cr-20Ni-4Mn sheet material after 1,000 h in humid air. The scale thickness is similar with some degree of Fe-rich oxide formed. In general, the surface oxides were very thin at this temperature and less characterization was performed.

Results at 700°C

Figure 6 shows specimen mass gain results for foil materials in 100 h cycles at 700°C in humid air. Similar results were observed as at 650°C with Fe-20Cr-20Ni-4Mn showing higher mass gains than the higher alloyed materials. The two curves for Fe-20Cr-20Ni-4Mn bracket the results for five foil specimens of this composition. One specimen is still running at 8,500 h while the others were stopped at 1,000, 2,000, 4,000 and 6,100 h to examine the reaction product and Cr depletion. At this temperature, the 347 foil specimen showed AAat ≈8,000 h and the 20/25/Nb specimen showed some nodule formation at ≈8,500 h. Specimens of alloy 120 and alloy 625 did not show any nodule formation after 10,000 h.

Increasing the reaction temperature from 650° to 700°C resulted in a thicker reaction product that was easier to characterize. Figure 7a shows the scale formed on a Fe-20Cr-20Ni-4Mn foil specimen after 1,000 h at 700°C in humid air. Compared to a sheet specimen of the model Fe-20Cr-20Ni+Mn,Si alloy, Figure 7b, the oxide is substantially thicker on Fe-20Cr-20Ni-4Mn and a significant amount of Mn-rich oxide formed with the higher Mn content. At longer times, precipitates (likely M_6C and $M_{23}C_6$)[4] develop in the metal along with a thicker scale, Figures 7c-7e. In order to further characterize these changes in the substrate and scale, EPMA maps were made of the entire foil specimen thickness after 4,000 h at 700°C, Figure 8. Few of the internal particles (as seen in Figure 7c) appear to be oxides, but

rather intermetallics (e.g. M_6C) rich in Cr, Mo and Si. Based on the Cr and Mn maps, Figures 8c and 8e, the scale appears to have an outer layer that is primarily MnO_x and an inner layer with a higher Cr content. As expected, there is some enrichment of Si near the alloy-scale interface indicating SiO_2 formation, Figure 8d. Composition profiles were made of this specimen as well as the Fe-20Cr-20Ni-4Mn specimen exposed for 2,000 h at 700°C, Figure 9. Rather than relying on mass change data, Cr profiles give explicit information about the amount of Cr being consumed. Unlike the results for 20/25/Nb foil specimens at 700°C, this material showed less Cr depletion at the substrate surface and a more uniform drop in Cr near the center of the specimen between 2,000 and 4,000 h, Figure 9a. These results suggest that the Cr diffusion may be relatively faster in this material or possibly that less Cr is being lost by evaporation from this material. The Mn content from the same set of profiles in Figure 9b shows an unusually severe Mn depletion in the alloy that is increasing with exposure time. The formation of a thick Mn-rich outer scale (suggested by Figure 8e) may be resulting in a large amount of Mn consumption. The Mn content in the center of both specimens appears to be higher than the starting Mn content. Rather than Mn becoming concentrated in the center, a more likely explanation is that a standard was not used for the normalization and there is overlap between the Cr and Mn peaks. This may have resulted in a problem calculating the absolute value of the Mn content.

Results at 800°C

Increasing the test temperature is commonly used in an attempt to accelerate the test to simulate long time exposures. Previous work[17,18] has suggested that this may be a questionable strategy for accelerating the evaluation process in this case, particularly since the higher temperature causes different water vapor effects than observed at lower temperature and allows more rapid Cr diffusion, thereby reducing Cr depletion on alloy grain boundaries. Nevertheless, oxidation data at 800°C has been useful in differentiating the performance of commercial foils, Figure 10, and model alloys, Figure 11. After less than 1,000 h at 800°C, a specimen of commercial 347 foil showed AA. In contrast, specimens of 20/25/Nb foil showed AA between 5,000 and 7,000 h, Figure 10. Analysis of the remaining Cr content showed a rapid increase in the rate of Cr consumption between specimens exposed for 5,000 and 6,000 h at 800°C in humid air.[5] A further increase in the Cr and Ni contents for alloy 120 resulted in only minor nodule formation after 10,000 h at 800°C. The Ni-base 625 specimen showed steady-state behavior with a minor mass loss due to Cr evaporation after a 6,000 h exposure. The general trend of improved AA resistance also was observed with sheet specimens of model alloys, Figure 11. For a constant 20%Ni content, the time to AA (indicated by a mass loss due to scale spallation with sheet specimens) increased with Cr content. Likewise, for a constant 20%Cr content, the time to AA increased with Ni content. The specimen of Fe-20Cr-25Ni has not shown AA after 3,900 h of exposure.

With these results as a framework, three Fe-20Cr-20Ni-4Mn foil specimens were tested at 800°C. One was removed at 1,000 h and the other two were stopped after 2,000 h at 800°C due to high mass gains, Figure 10. The mass gains after 2,000 h were as high as those observed for type 347 foil after 1,000 h. Figures 12a and 12b show the scale formed after 1,000 h at 800°C in humid air, and Figures 12c and 12d show the scale formed after 2,000 h where a significant amount of the metal has been consumed. Precipitates in the foil appear similar to those formed after exposure at 700°C. Similar to the results at 700°C, the scale formed on Fe-20Cr-20Ni-4Mn was thicker than that formed on Fe-20Cr-20Ni+Mn,Si, Figure 12e. This again suggests that the high Mn content increased the oxidation rate. One reason for pursuing this testing was that a sheet specimen of Fe-20Cr-20Ni-4Mn did not show AA until more than 5,000 h at 800°C in humid air. This value was twice as long as the Fe-20Cr-20Ni+Mn,Si specimen. However, after 6,000 h, a thick reaction product with a large amount of spallation was observed, Figure 12f. In this case, the larger substrate reservoir of Cr and Mn (due to its 0.8mm starting thickness compared to the 0.1mm thick foil specimen) may have resulted in a longer life despite the higher

oxidation rate. However, the faster oxidation rate appeared to be a critical problem for the foil specimens producing a disappointingly short lifetime at 800°C.

DISCUSSION

The improved creep and corrosion resistance shown by Fe-20Cr-20Ni-4Mn suggest that this base composition is a viable replacement candidate for type 347 stainless steel. However, this particular composition with 4%Mn may not be optimal. While the addition of Mn has been shown to be beneficial in reducing Cr evaporation in water-containing environments,[19] high levels of Mn in ferritic Fe-Cr alloys resulted in a higher isothermal oxidation rates with no benefit in air.[20] The 800°C results illustrate the problem with a thin-walled component. The Fe-20Cr-20Ni-4Mn specimen did not show AA like the 347 specimen; however, because of its rapid oxidation rate it still experienced a significant amount of metal loss in 2,000 h.

The results for Mn depletion at 700°C, Figure 9b, suggest that all of the Mn may have been consumed (i.e. oxidized) either in the surface scale or within the metal after 2,000 h at 800°C. Whether or not Mn depletion is a factor in the onset of AA has not been determined. However, the addition of both Mn and Si is needed to prevent AA in model alloys.[5] Furthermore, the higher Mn content in Fe-20Cr-20Ni-4Mn (compared to the model Fe-20Cr-20Ni alloy) resulted in an increased time to AA for sheet specimens at 800°C.[5] Another role of Mn may be to affect the Cr diffusion rate in the alloy. The Cr profiles presented in Figure 9a show less Cr depletion than other foil specimens exposed at the same temperature. More work needs to be done to confirm this effect. Manganese may be extremely beneficial in preventing AA at 650°C where Cr grain boundary depletion at the substrate surface appears to lead to localized AA.[17] To retard M_6C precipitation, B additions or higher C contents may be needed. If the Fe-20Cr-20Ni base composition is not sufficiently oxidation resistant in this application, the higher Ni content in Fe-20Cr-25Ni may be the next increment necessary to meet the program goals rather than going to the more expensive options of alloy 120 or alloy 625.

SUMMARY

Long-term oxidation results were presented for a developmental, corrosion-resistant Fe-20Cr-20Ni-4Mn alloy for replacing type 347 stainless steel foil in recuperators operating at 650°-700°C. This first attempt showed adequate creep strength and was resistant to accelerated attack at 650°-700°C in air with 10%H_2O. However, the relatively high Mn content resulted in an increased rate of oxidation at 700° and 800°C that may be detrimental for long-term behavior. A Mn-rich oxide may be beneficial for resistance to this environment but a thick oxide also may represent problems. The formation of M_6C precipitates after long-term exposures at 700° and 800°C also may be problematic. New alloys strengthened by different alloying strategies are now being processed for similar laboratory testing.

ACKNOWLEDGMENTS

The authors wish to thank J. D. Vought at ORNL for casting the alloys, G. W. Garner and J. Moser for performing the oxidation exposures, H. Longmire for performing the metallography and L. Walker for performing the microprobe work. P. F. Tortorelli and D. F. Wilson at ORNL reviewed the manuscript. The research was sponsored by the U.S. Department of Energy, Assistant Secretary for Energy Efficiency and Renewable Energy, Office of Distributed Energy, under contract DE-AC05-00OR22725 with UT-Battelle, LLC.

REFERENCES

1. B. A. Pint and J. M. Rakowski, NACE Paper 00-259, Houston, TX, presented at NACE Corrosion 2000, Orlando, FL, March 2000.
2. P. J. Maziasz and R. W. Swindeman, J. Eng. Gas Turbines and Power 125, (2003): pp.51-8.
3. J. M. Rakowski, ASME Paper #GT2003-38059, presented at the International Gas Turbine & Aeroengine Congress & Exhibition, Atlanta, GA, June 2-5, 2003.
4. P. J. Maziasz, R. W. Swindeman, J. P. Shingledecker, K. L. More, B. A. Pint, E. Lara-Curzio and N. D. Evans, Parsons 2003, Engineering Issues in Turbine Machinery, Power Plant and Renewables, A. Strang, et al. eds., Maney, London, 2003, pp.1057-73.
5. B. A. Pint, R. Peraldi and P. J. Maziasz, Mater. Sci. Forum 461-4, (2004): pp.799-806.
6. B. A. Pint and K. L. More, ASME Paper #GT2004-53627, presented at the International Gas Turbine & Aeroengine Congress & Exhibition, Vienna, Austria, June 14-17, 2004.
7. J. M. Rakowski, C. P. Stinner, M. Lipschutz and J. P. Montague, ASME Paper #GT2004-53917, presented at the International Gas Turbine & Aeroengine Congress & Exhibition, Vienna, Austria, June 14-17, 2004.
8. H. Asteman, J.-E. Svensson, M. Norell and L.-G. Johansson, Oxid. Met. 54, (2000): pp.11-26.
9. J. M. Rakowski and B. A. Pint, NACE Paper 00-517, Houston, TX, presented at NACE Corrosion 2000, Orlando, FL, March 2000.
10. J. M. Rakowski, ASME Paper 2001-GT-360, presented at the International Gas Turbine & Aeroengine Congress & Exhibition, New Orleans, LA, June 4-7, 2001.
11. B. A. Pint, NACE Paper 04-530, Houston, TX, presented at NACE Corrosion 2004, New Orleans, La, March 2004.
12. R. Peraldi and B. A. Pint, Oxid. Met. 61, (2004): pp.463-83.
13. I. Stambler, Gas Turbine World, Feb-Mar (2004): pp.12-16.
14. J. H. Watts, Global Gas Turbine News 39(1), (1999): pp.4-8.
15. M. Kikuchi, M. Sakakibara, Y. Otoguro, H. Mimura, S. Araki and T. Fujita, High Temperature Alloys, Their Exploitable Potential, J. B. Marriott, M. Merz, J. Nihoul and J. Ward eds., Elsevier, London, 1985, pp.267-76.
16. J. Kesseli, T. Wolf, J. Nash and S. Freedman, ASME Paper #GT2003-38938 presented at the International Gas Turbine & Aeroengine Congress & Exhibition, Atlanta, GA, June 2-5, 2003.
17. B. A. Pint, ASME Paper #GT2005-68495, to be presented at the International Gas Turbine & Aeroengine Congress & Exhibition, Reno-Tahoe, NV, June 6-9, 2005.
18. B. A. Pint, R. Peraldi and P. F. Tortorelli, NACE Paper 03-499, Houston, TX, presented at NACE Corrosion 2003, San Diego, CA, March 2003.
19. W. J. Quadakkers, T. Malkow, J. Piron-Abellan, U. Flesch, V. Shemet and L. Singheiser, Proc. 4th Eur. Solid Oxide Fuel Cell Forum, Vol. 2, A. J. McEvoy ed. (Elsevier, Amsterdam, 2000) p.827-36.
20. A. L. Marasco and D. J. Young, Oxid. Met. 36, (1991): pp.157-74.

TABLE 1

ALLOY CHEMICAL COMPOSITIONS (WEIGHT %) AND AVERAGE GRAIN SIZES (µm)

Material	Cr	Ni	Mn	Si	C	N	Nb	Ti	Mo	Other	average grain size
Type 347	17	11	1.6	0.6	0.04	0.02	0.6	0.04	0.1		5µm
Fe-20Cr-20Ni-4Mn	20.9	20.8	3.8	0.24	0.08	0.18	0.25	<	0.31	0.3 Cu, 0.3Co	55
										(foil)	10
Fe-16Cr-15Ni+MS	15.8	14.8	1.76	0.24	<	<	<	<	<		21
Fe-16Cr-20Ni+MS	15.8	19.7	1.72	0.24	0.003	0.001	<	<	<		26
Fe-20Cr-15Ni+MS	19.8	14.9	1.70	0.24	0.001	0.007	<	<	<		20
Fe-18Cr-17Ni+MS	17.8	17.6	1.63	0.25	0.001	0.002	<	<	<		27
Fe-18Cr-20Ni+MS	17.8	20.0	1.63	0.25	0.001	0.001	<	<	<		26
Fe-20Cr-17Ni+MS	19.8	17.6	1.62	0.26	0.001	0.001	<	<	<		21
Fe-20Cr-20Ni+MS	19.8	19.8	1.69	0.25	<	0.003	<	<	<		25
Fe-20Cr-25Ni+MS	19.8	25.0	1.64	0.25	<	0.001	<	<	<		23
20/25/Nb (Comm.)	20.3	24.7	1.03	0.38	0.064	0.161	0.23	0.04	1.51	0.05 Al	21
120	24.7	37.6	0.73	0.24	0.059	0.205	0.61	0.02	0.28	0.09 Al	24
625	26.0	63.6	0.04	0.23	0.019	0.042	0.17	0.17	8.90	0.18 Al,3.3 Fe	12

< indicates below the detectability limit of <0.01% or <0.001% for interstitials

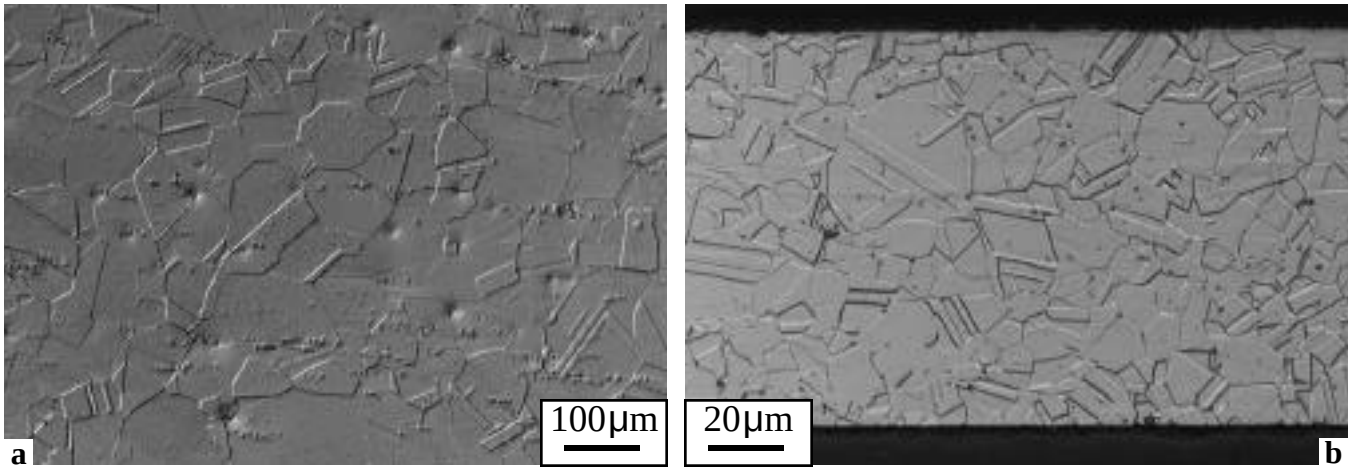

FIGURE 1. Light microscopy of Fe-20Cr-20Ni-4Mn (a) sheet material and (b) 100µm foil material.

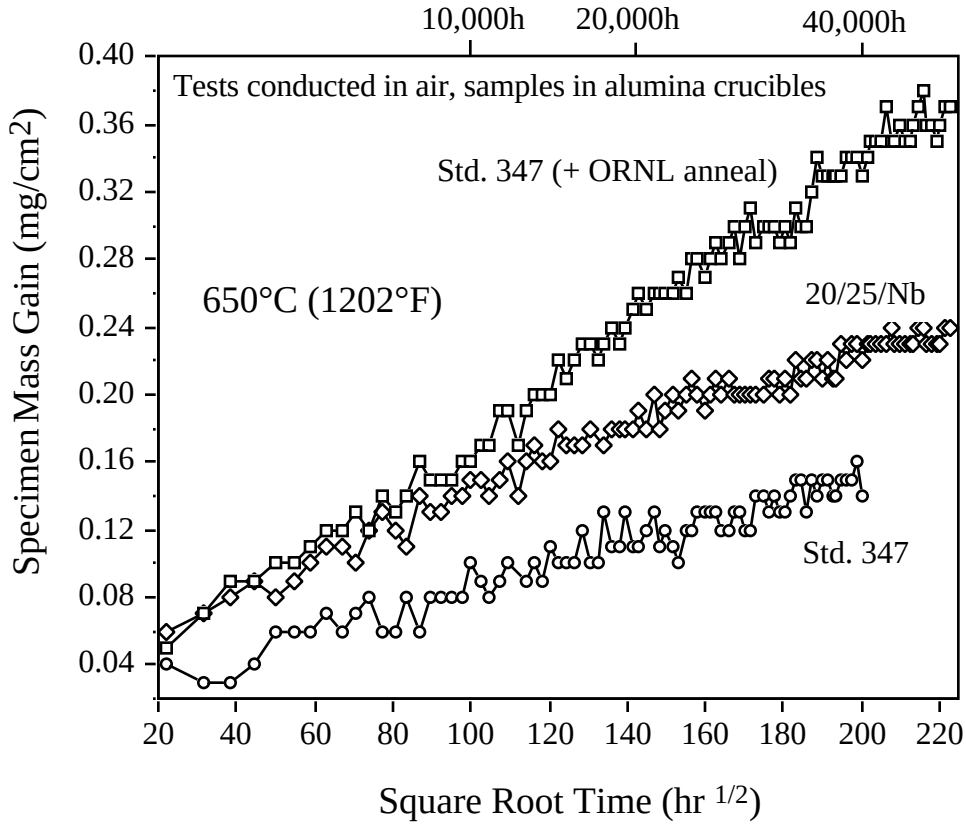

FIGURE 2. Specimen mass changes for commercial stainless steel foils in laboratory air during 500h cycles at 650°C plotted versus the square root of time to show the parabolic relationship.

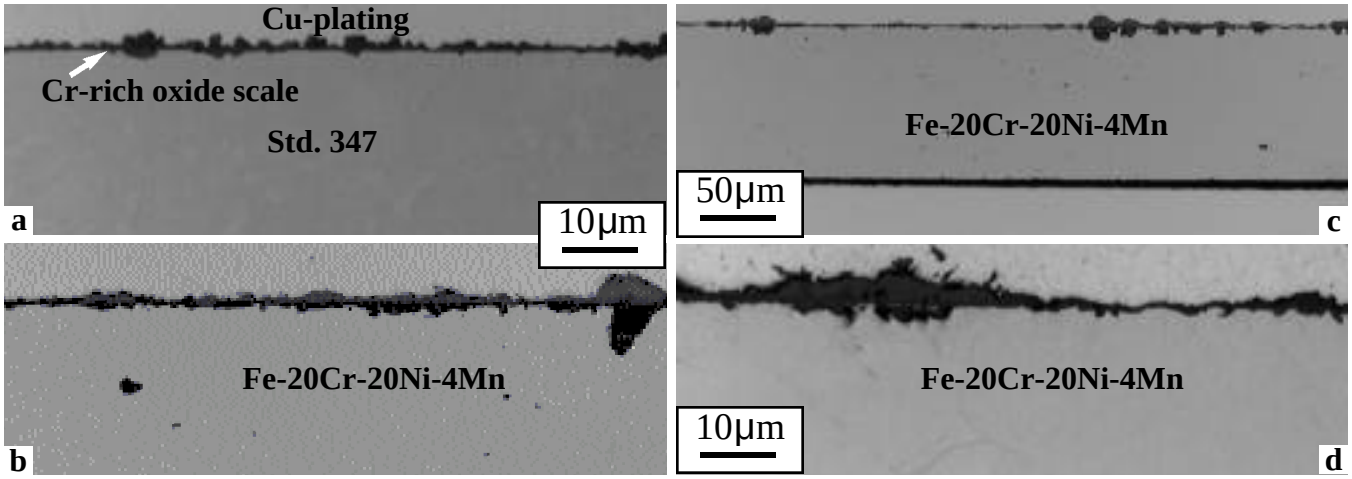

FIGURE 3. Light microscopy of polished cross-sections of specimens oxidized at 650°C (a) std 347 foil oxidized for 40,000 h in dry air, (b,c) Fe-20Cr-20Ni-4Mn foil oxidized for 1,000 h in humid air and (d) Fe-20Cr-20Ni-4Mn sheet material oxidized for 1,000 h in humid air.

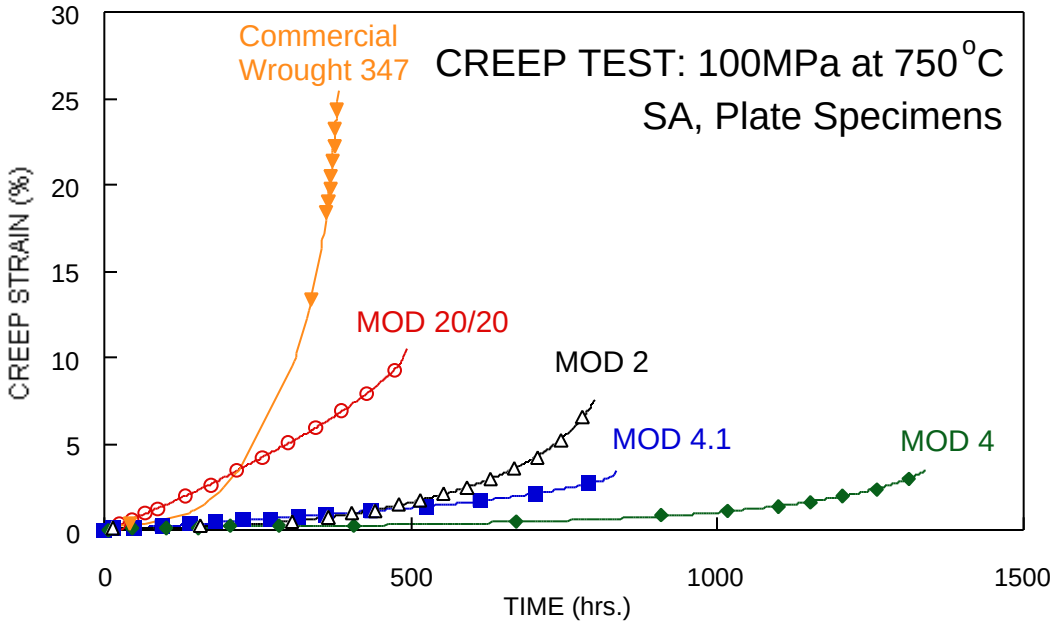

FIGURE 4. Creep results for various austenitic alloys tested at 100MPa and 750°C. The Fe-20Cr-20Ni-4Mn shows better creep strength than commercial type 347 material but not as good as modification of type 347.[2,4]

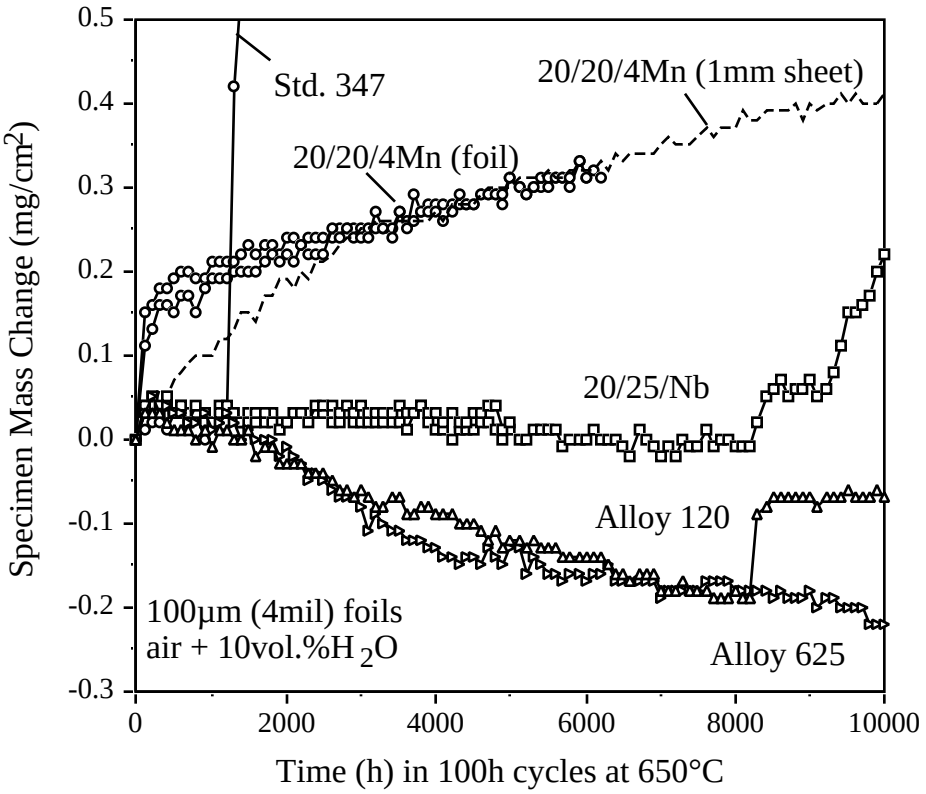

FIGURE 5. Specimen mass changes for foil specimens during 100 h cycles at 650°C in air plus 10%H_2O. For comparison, the mass gain for a sheet specimen of Fe-20Cr-20Ni-4Mn also is shown.

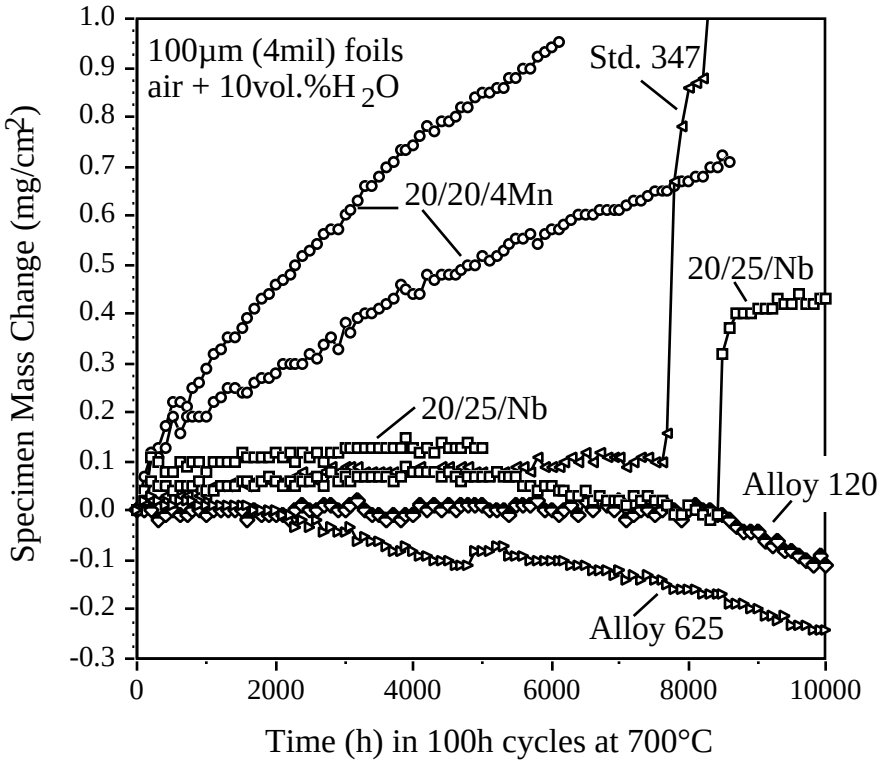

FIGURE 6. Specimen mass changes for foil specimens during 100 h cycles at 700°C in air plus 10%H_2O.

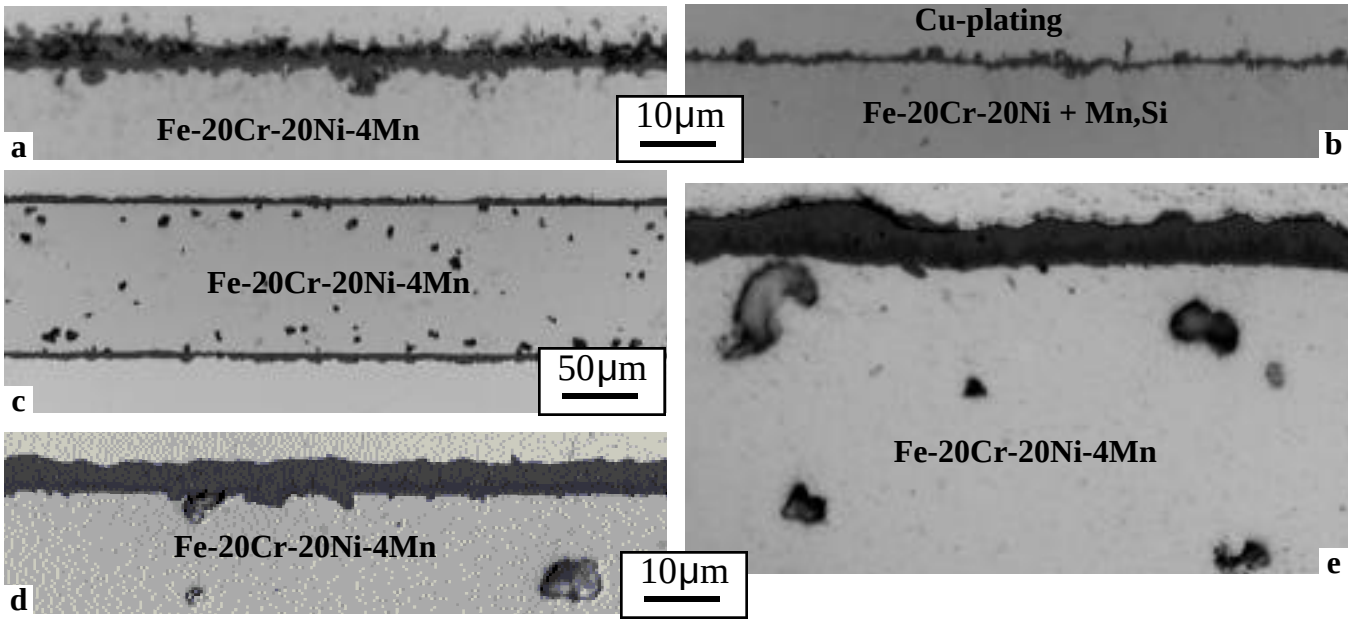

FIGURE 7. Light microscopy of polished cross-sections of specimens exposed at 700°C in humid air (a) Fe-20Cr-20Ni-4Mn for 1,000 h, (b) Fe-20Cr-20Ni+Mn,Si for 1,000 h, (c,d) Fe-20Cr-20Ni-4Mn for 4,000 h and (e) Fe-20Cr-20Ni-4Mn exposed for 6,100 h.

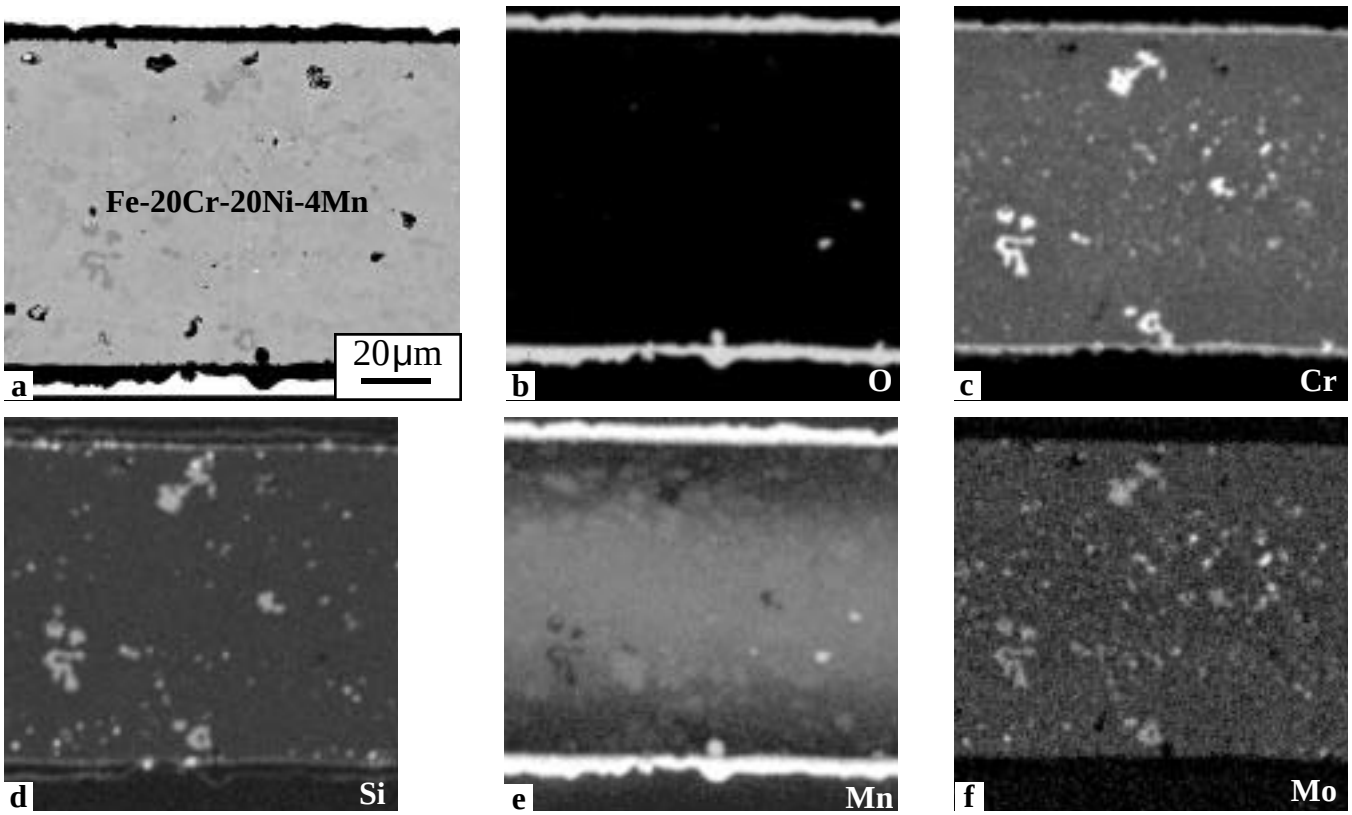

FIGURE 8. EPMAx-ray maps of the polished cross-section of Fe-20Cr-20Ni-4Mn after 4,000 h at 700°C in humid air shown in (a). Maps of (b) O, (c) Cr, (d) Si, (e) Mn and (f) Mo.

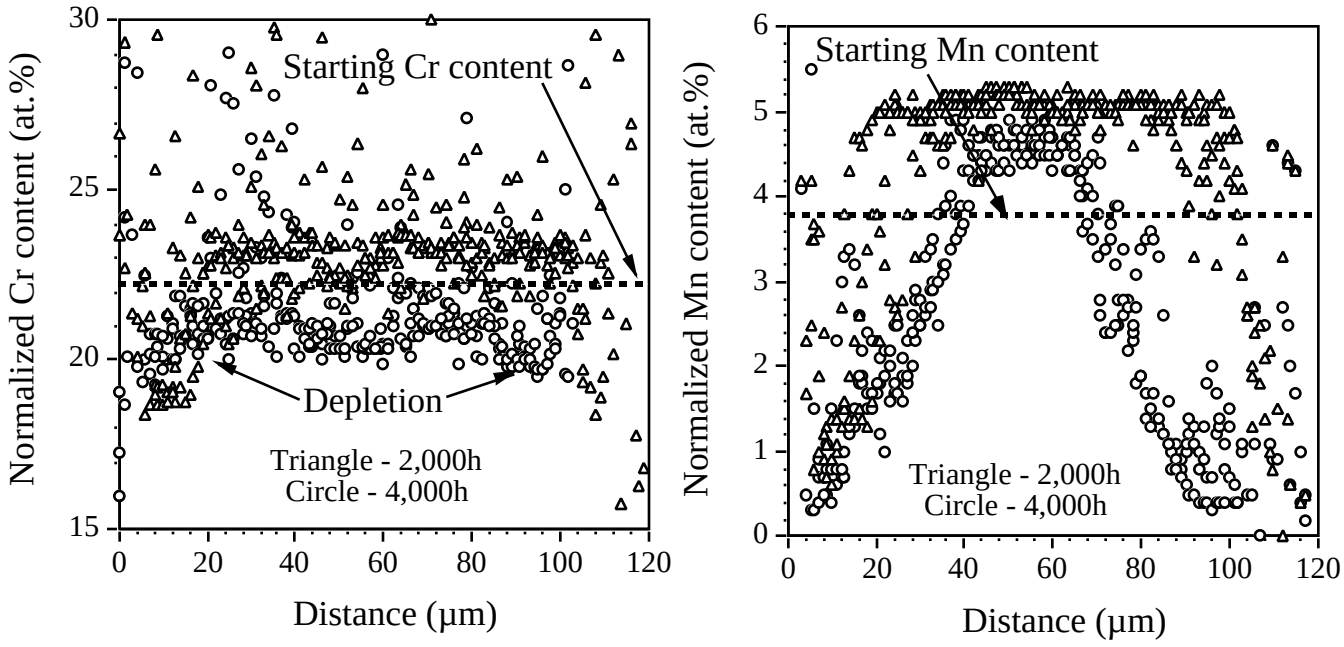

FIGURE 9. EPMA composition profiles from Fe-20Cr-20Ni-4Mn foil specimens exposed for 2,000 (triangles) and 4,000 h (circles) at 700°C in humid air, (a) Cr and (b) Mn. Three profiles for each specimen are shown.

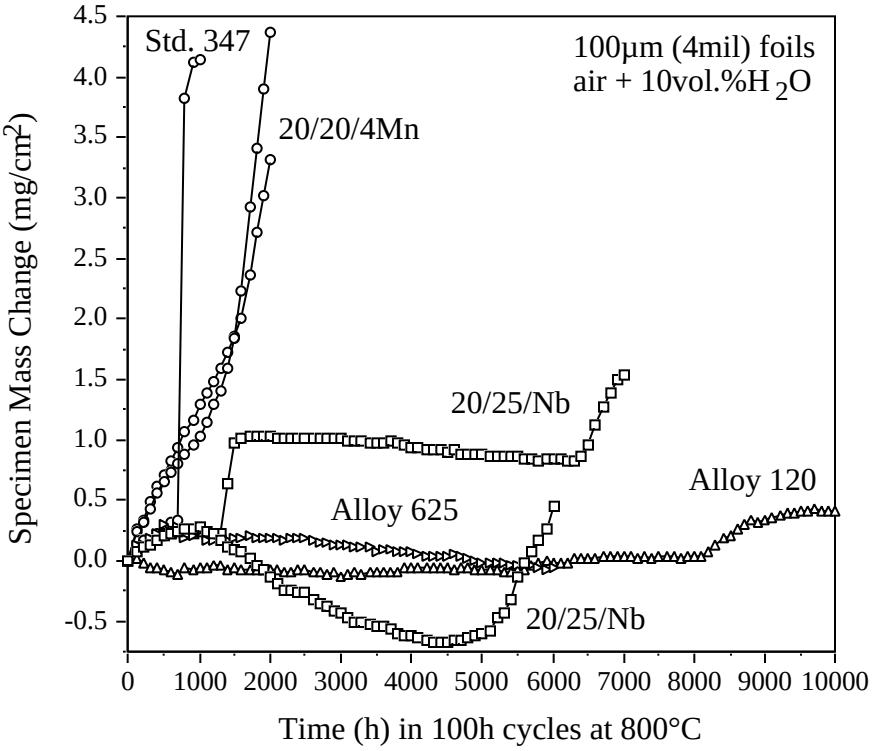

FIGURE 10. Specimen mass changes for foil specimens during 100 h cycles at 800°C in air plus 10%H_2O.

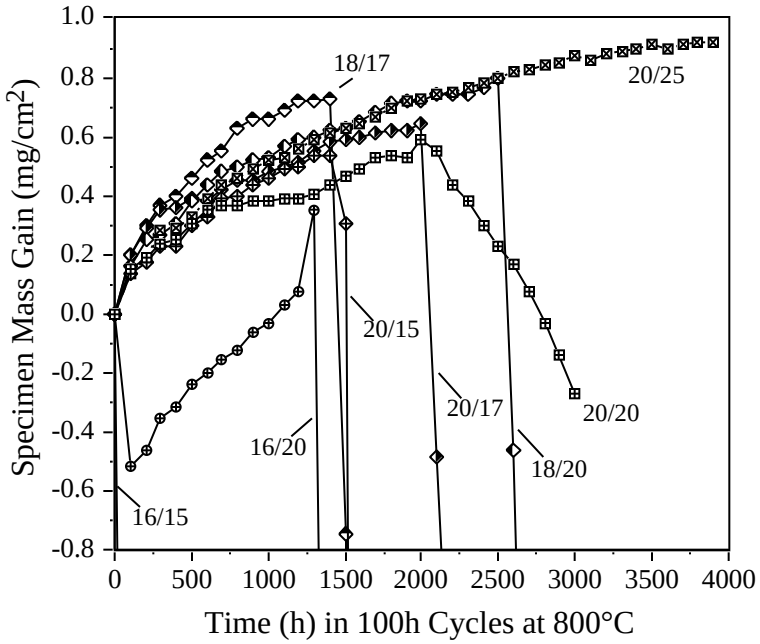

FIGURE 11. Specimen mass changes for model Fe-Cr-Ni alloys (specified by their Cr/Ni contents) during 100 h cycles at 800°C in air plus 10%H_2O. All contain additions of Mn and Si, Table 1.

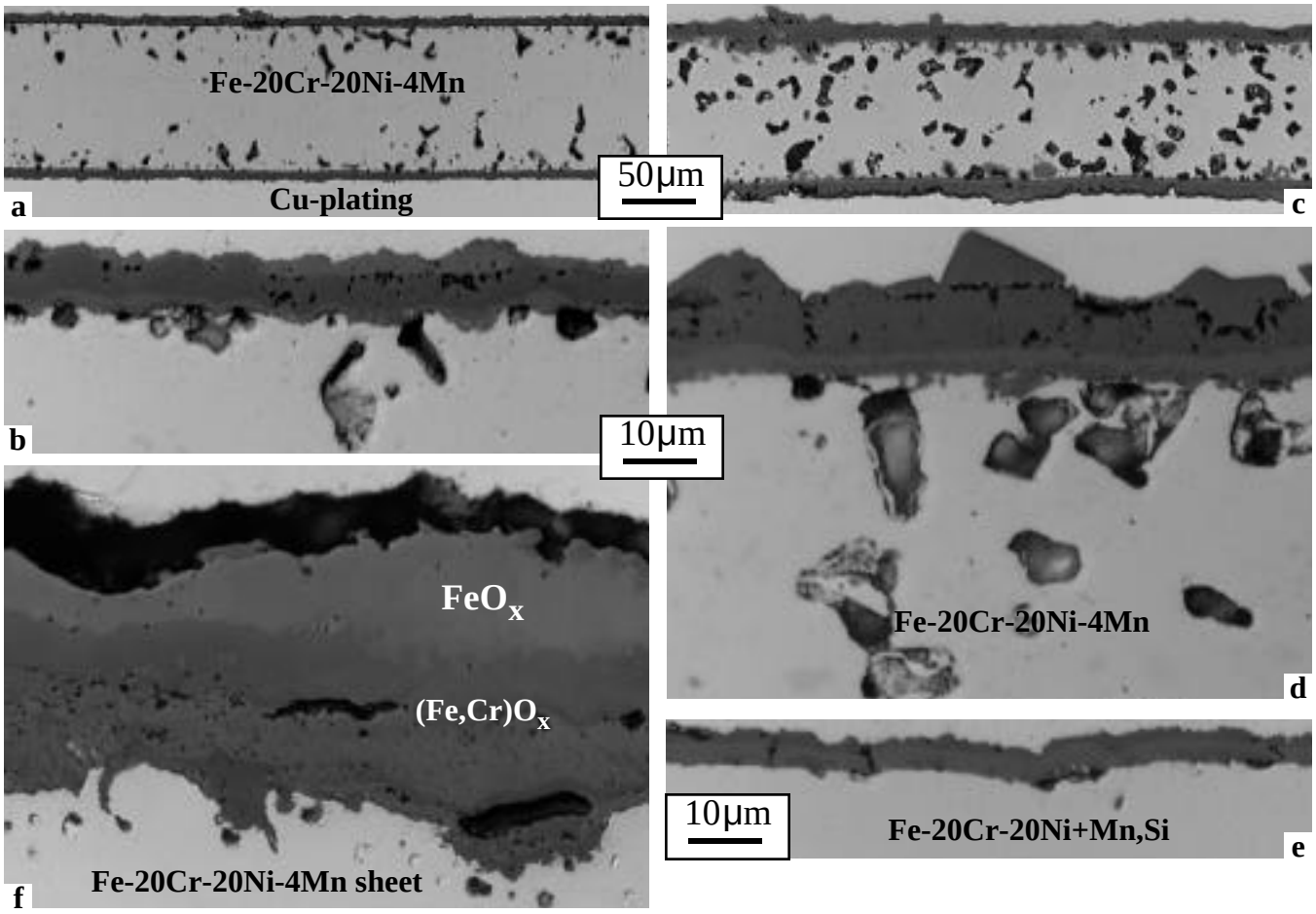

FIGURE 12. Light microscopy of polished cross-sections of Fe-20Cr-20Ni-4Mn foil oxidized at 800°C in humid air (a,b) foil after 1,000 h, (c,d) foil after 2,000 h, (e) Fe-20Cr-20Ni+Mn,Si after 1,000 h and (f) Fe-20Cr-20Ni-4Mn sheet after 6,000 h.